Phase transitions in the ferroelastic $[C_5H_{10}NH_2]SbCl_6$

2001 J. Phys.: Condens. Matter 13 6471

(http://iopscience.iop.org/0953-8984/13/30/303)

INSTITUTE OF PHYSICS PUBLISHING JOURNAL OF PHYSICS: CONDENSED MATTER

J. Phys.: Condens. Matter **13** (2001) 6471–6488 PII: S0953-8984(01)21816-5

Phase transitions in the ferroelastic $[C_5H_{10}NH_2]SbCl_6$

A Pietraszko[1], B Bednarska-Bolek[2], R Jakubas[2] and P Zieliński[3]

[1] Institute of Low Temperature and Structure Research of the Polish Academy of Science, Okólna 2, 50-422 Wrocław, Poland
[2] Faculty of Chemistry, University of Wrocław, F Joliot Curie 14, 50-383 Wrocław, Poland
[3] H Niewodniczański Institute of Nuclear Physics, 31-342 Kraków, Poland

Received 9 February 2001, in final form 18 May 2001
Published 13 July 2001
Online at stacks.iop.org/JPhysCM/13/6471

Abstract

A new piperidinium chloroantimonate-(v) analogue, $(C_5H_{10}NH_2)SbCl_6$ has been studied by means of single-crystal x-ray diffraction, differential scanning calorimetry, thermal expansion and dielectric techniques. It undergoes three solid–solid state phase transitions: at 363 K first order (from $Cmcm$ (phase I) to Cc (phase II)), at 310 K second order (from Cc to $P1$ (phase III)) and at 283 K first order (from $P1$ to $P2_1/m$ (phase IV)). The crystal structure of $(C_5H_{10}NH_2)SbCl_6$ has been solved at 293 K (phase III) and at 338 K (phase II). It consists of isolated $SbCl_6^-$ anions and piperidinium cations. The ferroelastic domain structure appears below 363 K. Group theoretical analysis of phase transitions is presented.

(Some figures in this article are in colour only in the electronic version; see `www.iop.org`)

1. Introduction

Alkylammonium halogenoantimonates (III) and bismuthates (III) of general formula $R_aM_bX_{3b+a}$ (where R is an organic cation; M = Sb^{+3}, Bi^{+3}; X = Cl, Br, I) are attracting growing attention since many salts of this group reveal ferroelectric and ferroelastic properties [1–3]. They are molecular, ionic crystals with anionic sublattices composed of deformed MX_6 octahedra either isolated or connected with neighbouring octahedra by corners, edges or faces. The alkylammonium cations located in the anionic cavities are believed to be responsible for the ferroelectric ordering in the low-temperature phases [4–6].

While the chloroantimonates (v) were synthesized nearly hundred years ago, very little is known about their physical properties, in particular about their possible phase transitions in solid state. The characteristic feature of halogenoantimonate (v) ionic crystals of the general formula $RSbCl_6$ ((R denotes an organic cation), as distinguished from the antimonates (III)), is that the octahedral units are all isolated in the crystal lattice. We have recently reported that several compounds belonging to the $RSbCl_6$ family exhibit interesting ferroic (ferroelastic) properties. Four ferroic $RSbCl_6$ crystals have been discovered up to now: $[P(CH_3)_4]SbCl_6$ [7], $[C(NH_2)_3]SbCl_6$ [8] and $(C_5H_{10}NH_2)SbCl_6 \cdot (C_5H_{10}NH_2)Cl$ [9] and $[(C_2H_5)_3NH]SbCl_6$ [10]. The structure of these salts is quite simple and consists of isolated $SbCl_6^-$ anions and organic

cations. In the case of piperidinium salt having more complicated stoichiometry, $RSbCl_6 \cdot RCl$, the crystal lattice also contains an isolated Cl^- ion. The mechanism of the phase transitions seems to be complex, because the dynamics of both sublattices, anionic and cationic, may be involved in it. Most of the phase transitions exhibit an order–disorder character. It is interesting that the ferroic properties in the $RSbCl_6$ family of crystals are encountered in crystals having small organic cations. During the synthesis of piperidinium chloroantimonates (v) analogues, apart from the mentioned $(C_5H_{10}NH_2)SbCl_6 \cdot (C_5H_{10}NH_2)Cl$ crystals we were able to obtain a new ferroelastic compound having simpler stoichiometry (1:1) namely, $(C_5H_{10}NH_2)SbCl_6$ (abbreviated PCA).

In the present work we report x-ray at 293 and 338 K, differential scanning calorimetry (DSC), dilatometric, dielectric and optical results of the PCA crystals. A comparison of PCA with other $RSbCl_6$ ferroic crystals is made. A group theoretical analysis of phase transitions in PCA is presented.

2. Experimental details

$(C_5H_{10}NH_2)SbCl_6$ was prepared by reacting $(C_5H_{10}NH_2)Cl$ and $SbCl_5$ (molar ratio 1:1) in concentrated hydrochloric acid. The single crystals were grown by the evaporation method at room temperature from an ethanol solution.

Table 1. Crystal data and structure refinement for PCA.

	293 K	338 K
Identification code		$(C_5H_{10}NH_2)SbCl_6$
Empirical formula		C5 H12 Cl6 N Sb
Formula weight		420.61
Temperature	293(2) K	338(2) K
Wavelength	0.710 73 Å	0.710 73 Å
Crystal system, space group	Triclinic, $P1$	Monoclinic, Cc
Unit cell dimensions	$a = 8.013(2)$ Å $\alpha = 89.51(3)^\circ$	$a = 7.999(2)$ Å $\alpha = 90^\circ$
	$b = 8.042(2)$ Å $\beta = 70.58(3)^\circ$	$b = 22.569(5)$ Å$\beta = 96.40(3)^\circ$
	$c = 11.917(2)$ Å $\gamma = 82.97(3)^\circ$	$c = 8.139(2)$ Å $\gamma = 90^\circ$
Volume	718.4(3) Å^3	1460.2(6) Å^3
Z, Calculated density	2, 1.944 Mg m^{-3}	4, 1.913 Mg m^{-3}
Absorption coefficient	2.999 mm^{-1}	2.951 mm^{-1}
$F(000)$	404	808
Crystal size	0.26 × 0.18 × 0.09 mm	0.26 × 0.18 × 0.09 mm
θ-range for data collection	5.11–26.37°	5.13–25.66°
Limiting indices	$-10 \leqslant h \leqslant 9$, $-9 \leqslant k \leqslant 10$, $-141 \leqslant l \leqslant 14$	$-9 \leqslant h \leqslant 9$, $-27 \leqslant k \leqslant 27$, $-9 \leqslant l \leqslant 9$
Reflections collected/unique	3896/3194 (R(int) = 0.0333)	3552/1782 (R(int) = 0.0285)
Completeness to theta = 26.37	89.5%	98.1%
Refinement method	Full-matrix least-squares on F^2	Full-matrix least-squares on F^2
Data/restraints/parameters	3194/3/308	1782/8/166
Goodness-of-fit on F^2	1.411	1.195
Final R indices ($I > 2\sigma(I)$)	$R_1 = 0.0468$, $wR_2 = 0.0928$	$R_1 = 0.0501$, $wR_2 = 0.1039$
R indices (all data)	$R_1 = 0.0525$, $wR_2 = 0.0987$	$R_1 = 0.0587$, $wR_2 = 0.1124$
Extinction coefficient	0.0001	0.004 64(18)
Largest diff. peak and hole	0.938 and −0.780 e Å^{-3}	0.885 and −0.581e Å^{-3}

DSC measurements were carried out using a Perkin-Elmer DSC-7 calorimeter. The DSC measurements were performed with cooling/heating rates ranging from 3 to 20 K min^{-1}.

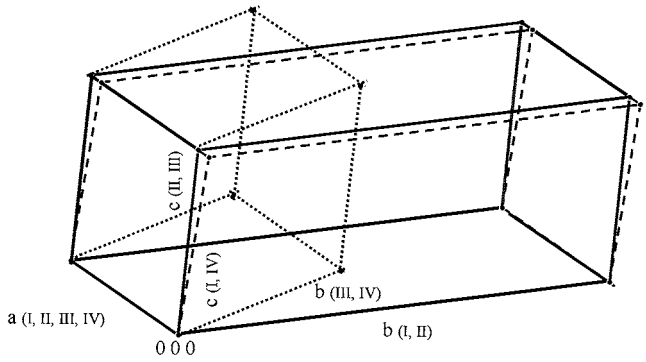

Figure 1. Transformation between different unit cells of PCA characterizing the orthorhombic (I) → monoclinic(II) → triclinic(III) → monoclinic (IV) transitions.

The linear thermal expansion was measured using a thermomechanical analyser Perkin-Elmer TMA-7. The samples used in the measurements were prepared in the form of plate of dimensions $5 \times 5 \times 2$ mm^3. The dilatometric measurements were performed in heating and cooling runs at a rate of 1.5 K min^{-1}. The accuracy of the thermal expansion determination was about 5%.

The complex electric permittivity, ε^*, was measured using HP 4285A Precision LCR meter in the frequency range between 75 kHz and 30 MHz and in the temperature region 250–380 K. The measurements were performed with a cooling/heating rate of 0.5 K min^{-1} in the vicinity of the phase transitions and 2 K min^{-1}, elsewhere. Samples of typical dimensions of $5 \times 5 \times 1$ mm^3 taken as a single-crystal thin plates were silver painted. The overall error for the real and imaginary parts of the complex electric permittivity was less than 5%.

A crystal with dimensions $0.09 \times 0.18 \times 0.26$ mm^3 was mounted on a Kuma diffraction single-crystal diffractometer equipped with a two-dimension area CCD detector. Mo Kα graphite monochromated radiation and an ω scan, with $\Delta\omega = 75^\circ$ for one image, were used for data collection. 960 images for six different runs covered 93% of the Ewald sphere. The crystal data and experimental details are given in table 1. The lattice parameters calculated using about 150 reflections obtained from 30 images for 10 runs with different orientations in reciprocal space. The temperature measurements in the 175–320 K range were performed using an Oxford Cryostream Cooler by a stream of cold nitrogen with an accuracy of stability of the temperature of ± 0.5 K. In the high-temperature range the attachment of Kuma diffraction with a hot air stream allowed us to control the temperature with the accuracy of ± 0.3 K.

The structure was solved by a heavy-atom method and subsequently by the difference Fourier syntheses SHELXTL_PLUS program system (GM Sheldrick of SHELXL) [11]. The structure refinement by a full matrix, least-squares method on (F_0^2) was done using SHELXL97 [12]. Anisotropic thermal displacement parameters were used for all non-hydrogen atoms. The hydrogen atoms were located in the difference Fourier maps.

3. Results

3.1. X-ray data

The temperature dependent x-ray measurements showed that PCA crystal possesses a rich polymorphism exhibiting several phases between 100 and 400 K. The four crystalline phases of PCA are denoted successively as I, II, III and IV, starting from the phase existing above 369 K.

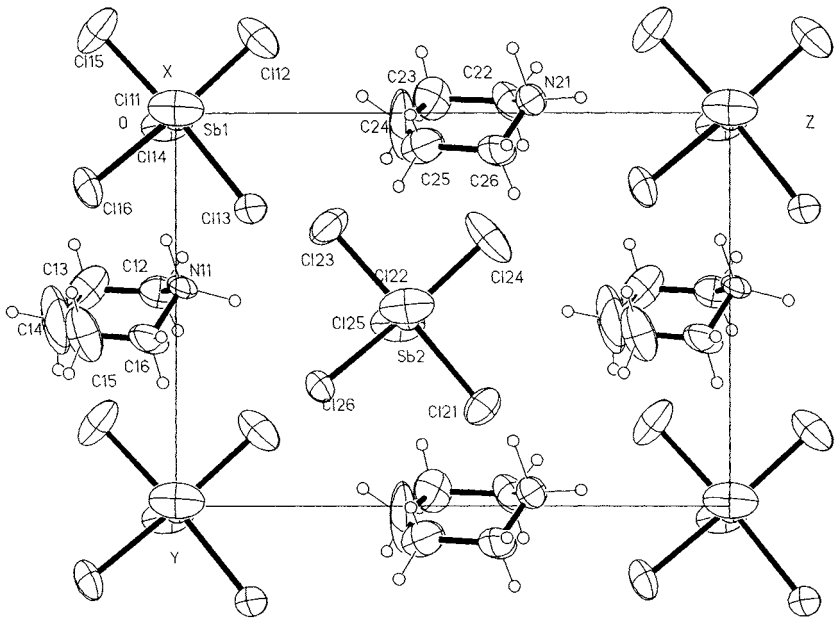

Figure 2. Projection of the crystal structure of PCA onto the *b–c* plane at 293 K (phase III).

The transformation matrix of the unit cell from phase IV (and phase III) to phase II and phase I is the following:

$$\begin{pmatrix} -1 & 0 & 0 \\ 1 & 0 & 2 \\ 0 & -1 & 0 \end{pmatrix}.$$

The transformation between different unit-cells of PCA is illustrated in figure 1. The crystal structures have been determined successfully for phases III and II. After cooling below 283 K the sample usually cracks as a result of large distortions of the crystal lattice when the phase transition is crossed. A similar situation during the heating of the sample takes place at about $T_c = 369$ K. At room temperature the crystal structure of PCA belongs to the triclinic system with the space group $P1$. The statistical distribution of $|E|$ values, compared with theoretical values expected for the centrosymmetric and acentric space group gave an indication of the acentric structure. The refinement of the crystal structure for both space groups $P\bar{1}$ and $P1$ confirmed the acentric symmetry. The unit cell of phase III contains two independent $SbCl_6$ groups and the two piperidinium groups. The projections of the crystal structure of PCA onto the *b–c* plane at 293 K (phase III) is shown in figure 2. Details of the molecular structure geometry are given in tables 2 and 3. The piperidinium groups having a chair conformation are ordered but the anisotropic displacement amplitudes of the N and one of the C atoms are relatively large. The weak hydrogen bonds of N–H . . . Cl have been found at room temperature (see table 4). These relatively weak but specific interactions between $SbCl_6$ and piperidinium molecules seem to play an important role in the mechanism of the phase transitions.

The crystal structure of phase II belongs to the monoclinic system (Cc space group). The projection of the structure onto the *a–b* plane at 338 K (phase II) is shown in the figure 3. Examination of the structural arrangement of the piperidinium groups shows that these cations exhibited very large displacement factors for the N(1) and for the other C atoms of this ring, particularly in the *a–b* plane. The piperidinium ring seems to have a twisted boat conformation.

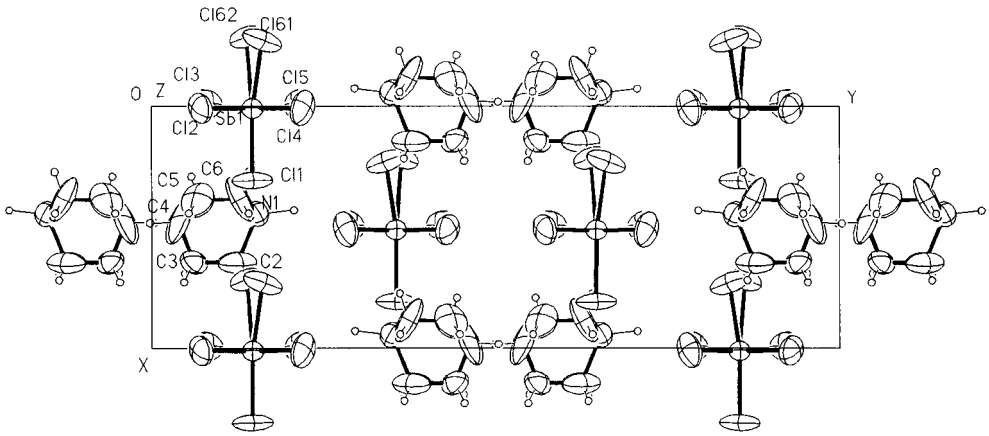

Figure 3. Projection of the crystal structure of PCA onto the *a*–*b* plane at 338 K (phase II).

Table 2. Atomic coordinates ($\times 10^{-4}$) and equivalent isotropic displacement parameters ($A^2 \times 10^3$) for phases II and III. $U_{(eq)}$ is defined as one-third of the trace of the orthogonalized U_{ij} tensor.

	293 K					338 K			
	x	*y*	*z*	$U_{(eq)}$		*x*	*y*	*z*	$U_{(eq)}$
Sb(1)	−57(1)	39(1)	3(1)	58(1)	Sb(1)	103(1)	1457(1)	−2(1)	89(1)
Cl(11)	2886(2)	−139(2)	11(2)	120(1)	Cl(1)	3063(2)	1455(1)	175(2)	172(1)
Cl(12)	−697(3)	−1928(3)	1492(2)	129(1)	Cl(2)	79(3)	708(1)	2020(3)	167(1)
Cl(13)	−982(2)	2422(2)	1348(1)	75(1)	Cl(3)	−88(3)	766(1)	−2105(3)	208(1)
Cl(14)	−2950(2)	277(2)	−152(2)	108(1)	Cl(4)	−85(3)	2151(1)	−2125(3)	170(1)
Cl(15)	755(3)	−2134(3)	−1391(2)	137(1)	Cl(5)	71(3)	2186(1)	2067(2)	165(1)
Cl(16)	803(2)	1879(2)	−1568(1)	107(1)	Cl(61)	−2714(5)	1601(3)	−231(6)	180(2)
Sb(2)	2796(1)	5114(1)	4157(1)	59(1)	Cl(62)	−2860(4)	1374(2)	−287(4)	138(1)
Cl(21)	1902(2)	7461(2)	5529(1)	91(1)	N(1)	4435(7)	1521(2)	4408(6)	113(2)
Cl(22)	5759(2)	4900(2)	4164(2)	116(1)	C(2)	6450(9)	1231(5)	4452(11)	180(4)
Cl(23)	3644(3)	2878(2)	2755(2)	127(1)	C(3)	6425(9)	602(3)	4441(10)	146(3)
Cl(24)	2200(3)	3160(3)	5643(2)	153(1)	C(4)	4785(14)	386(2)	4851(18)	253(3)
Cl(25)	−55(2)	5342(2)	3998(2)	119(1)	C(5)	3866(13)	662(4)	5730(12)	200(4)
Cl(26)	3740(3)	6948(2)	2594(1)	105(1)	C(6)	3836(12)	1273(3)	5642(9)	202(3)
N(11)	5563(5)	4404(4)	114(3)	59(1)					
C(12)	3866(7)	4536(7)	−304(5)	83(2)					
C(13)	4373(8)	4445(10)	−1583(6)	116(2)					
C(14)	6000(20)	5239(19)	−2140(7)	279(8)					
C(15)	7123(8)	5601(11)	−1643(6)	127(3)					
C(16)	6636(9)	5726(7)	−485(5)	103(2)					
N(21)	7036(6)	−336(6)	6413(3)	79(1)					
C(22)	5412(9)	−295(9)	6027(5)	101(2)					
C(23)	6001(9)	−372(11)	4628(6)	107(3)					
C(24)	7603(16)	275(14)	4089(6)	270(5)					
C(25)	8729(11)	835(9)	4456(7)	148(3)					
C(26)	8118(10)	953(8)	5797(6)	108(3)					

In the anionic $SbCl_6$ group the disordered configuration has been found for the Cl(6) atom. Comparison of the distances in the N–Cl and C–Cl atoms shows that the hydrogen bonds (see table 4) are very weak and probably do not play a significant role in the packing of molecules.

Table 3. Selected bond lengths (Å) and angles (°) for phases II and III.

293 K		338 K	
Sb(1)–Cl(15)	2.299(2)	Sb(1)–Cl(61)	2.263(4)
Sb(1)–Cl(12)	2.337(2)	Sb(1)–Cl(3)	2.308(3)
Sb(1)–Cl(16)	2.3480(16)	Sb(1)–Cl(4)	2.324(2)
Sb(1)–Cl(11)	2.3485(17)	Sb(1)–Cl(1)	2.3558(17)
Sb(1)–Cl(14)	2.3704(16)	Sb(1)–Cl(5)	2.3556(19)
Sb(1)–Cl(13)	2.3898(15)	Sb(1)–Cl(2)	2.362(2)
Sb(2)–Cl(24)	2.325(2)	Sb(1)–Cl(62)	2.363(4)
Sb(2)–Cl(25)	2.3394(17)	Cl(61)–Cl(62)	0.528(8)
Sb(2)–Cl(23)	2.342(2)	N(1)-C(6)	1.288(9)
Sb(2)–Cl(26)	2.3465(16)	N(1)-C(2)	1.736(9)
Sb(2)–Cl(22)	2.3615(17)	C(2)-C(3)	1.420(12)
Sb(2)–Cl(21)	2.3855(18)	C(3)-C(4)	1.472(13)
N(11)-C(16)	1.477(7)	C(4)-C(5)	1.249(15)
N(11)-C(12)	1.589(7)	C(5)-C(6)	1.381(12)
C(12)-C(13)	1.440(9)	Cl(61)–Sb(1)–Cl(3)	93.04(15)
C(13)-C(14)	1.472(17)	Cl(61)–Sb(1)–Cl(4)	82.01(16)
C(14)-C(15)	1.291(18)	Cl(3)–Sb(1)–Cl(4)	84.88(10)
C(15)-C(16)	1.304(9)	Cl(61)–Sb(1)–Cl(1)	171.79(16)
N(21)-C(26)	1.465(8)	Cl(3)–Sb(1)–Cl(1)	91.54(9)
N(21)-C(22)	1.514(9)	Cl(4)–Sb(1)–Cl(1)	91.63(9)
C(22)-C(23)	1.575(9)	Cl(61)–Sb(1)–Cl(5)	82.46(15)
C(23)-C(24)	1.393(13)	Cl(3)–Sb(1)–Cl(5)	175.33(9)
C(24)-C(25)	1.255(15)	Cl(4)–Sb(1)–Cl(5)	93.22(7)
C(25)-C(26)	1.508(11)	Cl(1)–Sb(1)–Cl(5)	92.78(8)
Cl(15)–Sb(1)–Cl(12)	88.64(7)	Cl(61)–Sb(1)–Cl(2)	94.28(16)
Cl(15)–Sb(1)–Cl(16)	88.27(7)	Cl(3)–Sb(1)–Cl(2)	91.59(8)
Cl(12)–Sb(1)–Cl(16)	175.42(6)	Cl(4)–Sb(1)–Cl(2)	174.71(8)
Cl(15)–Sb(1)–Cl(11)	90.49(8)	Cl(1)–Sb(1)–Cl(2)	92.40(8)
Cl(12)–Sb(1)–Cl(11)	90.27(8)	Cl(5)–Sb(1)–Cl(2)	90.00(8)
Cl(16)–Sb(1)–Cl(11)	86.38(8)	Cl(61)–Sb(1)–Cl(62)	12.87(19)
Cl(15)–Sb(1)–Cl(14)	87.77(8)	Cl(3)–Sb(1)–Cl(62)	83.70(12)
Cl(12)–Sb(1)–Cl(14)	93.48(8)	Cl(4)–Sb(1)–Cl(62)	89.99(12)
Cl(16)–Sb(1)–Cl(14)	89.78(7)	Cl(1)–Sb(1)–Cl(62)	174.82(12)
Cl(11)–Sb(1)–Cl(14)	175.83(7)	Cl(5)–Sb(1)–Cl(62)	92.04(12)
Cl(15)–Sb(1)–Cl(13)	175.67(7)	Cl(2)–Sb(1)–Cl(62)	85.71(11)
Cl(12)–Sb(1)–Cl(13)	94.98(6)	Cl(62)–Cl(61)–Sb(1)	94.3(6)
Cl(16)–Sb(1)–Cl(13)	88.26(5)	Cl(61)–Cl(62)–Sb(1)	72.8(6)
Cl(11)–Sb(1)–Cl(13)	91.89(7)		
Cl(14)–Sb(1)–Cl(13)	89.62(6)		
Cl(24)–Sb(2)–Cl(25)	94.36(8)		
Cl(24)–Sb(2)–Cl(23)	88.15(8)		
Cl(25)–Sb(2)–Cl(23)	88.11(8)		
Cl(24)–Sb(2)–Cl(26)	173.45(8)		
Cl(25)–Sb(2)–Cl(26)	91.43(8)		
Cl(23)–Sb(2)–Cl(26)	88.98(6)		
Cl(24)–Sb(2)–Cl(22)	88.97(9)		
Cl(25)–Sb(2)–Cl(22)	175.79(7)		
Cl(23)–Sb(2)–Cl(22)	89.42(9)		
Cl(26)–Sb(2)–Cl(22)	85.11(8)		
Cl(24)–Sb(2)–Cl(21)	93.88(7)		
Cl(25)–Sb(2)–Cl(21)	90.68(7)		
Cl(23)–Sb(2)–Cl(21)	177.72(7)		
Cl(26)–Sb(2)–Cl(21)	89.11(6)		
Cl(22)–Sb(2)–Cl(21)	91.67(7)		

Table 4. Hydrogen bonds for phase III.

D–H . . . A	d(D–H)	d(H . . . A)	d(D . . . A)	⟨(DHA)
N(11)–H(11A) . . . Cl(14)[a]	1.02(4)	2.39(4)	3.367(4)	161(3)
N(11)–H(11B) . . . Cl(26)	1.10(3)	2.43(3)	3.398(4)	146(3)

[a] The symmetry transformations used to generate equivalent atoms were $x + 1, y, z$.

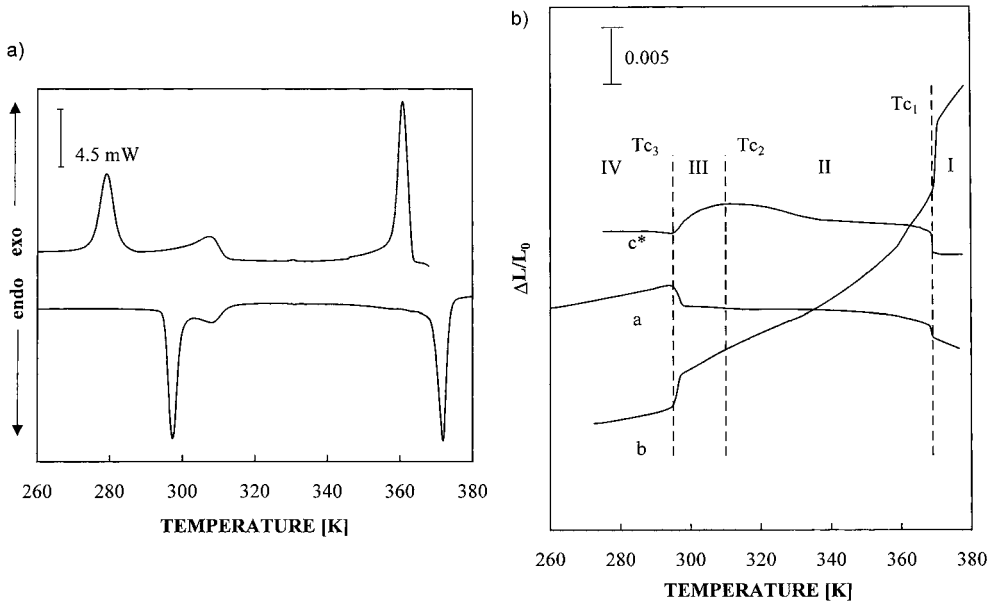

Figure 4. (a) DSC curves obtained on heating and cooling for PCA (scanning rate 5 K min^{-1}, sample mass 34.220 mg), (b) temperature dependence of the linear thermal expansion $\Delta L/L_0$ of the PCA crystal along the a-, b- and c-directions during heating.

3.2. DSC and dilatometric measurements

Three thermal anomalies were detected in the temperature range 260–380 K during the first and second DSC scans (see figure 4(a)). These effects are well reversible in the cooling and heating cycles. Powdering of the sample does not influence the shape of the heat anomalies. The thermal hysteresis was estimated from the scans performed at various rates extrapolated to a scanning rate of 0 K min^{-1}. Strong heat anomalies and large thermal hysteresis indicate the first-order character of the I → II and III → IV phase transitions. Results of the calorimetric studies of PCA are collected in table 5.

The overall behaviour of the linear thermal expansion of PCA single crystal along all the crystallographic directions in the heating scans is shown in figure 4(b) (the directions presented correspond to those taken for the triclinic phase). One can state that the sequence of the phase transitions revealed by the dilatometric measurements is consistent with that found by the DSC studies. It is clearly seen that both the first-order phase transitions, I → II and III → IV, are accompanied by a strong jump in dilation for all axes. This accounts for the breaking of single crystals at these points. The apparently continuous phase transition II → III at 310 K is hardly visible in dilation ($\Delta L/L_0$) for the a- and b-axes, whereas a clear maximum of the $\Delta L/L_0(T)$ curve for the c^*-direction is observed (the c^*-direction is perpendicular to the a–b plane). However, the phase transition is accompanied by a strong shear related with the angle α.

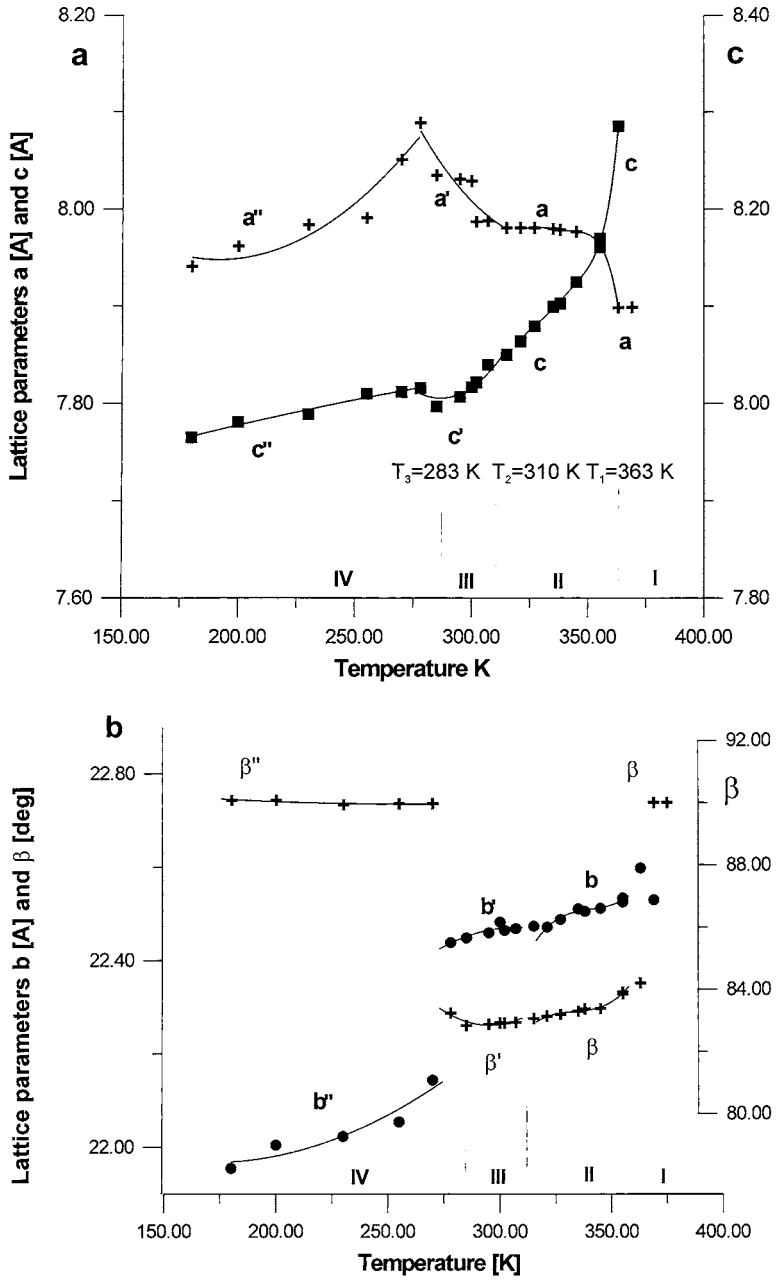

Figure 5. Experimental values of (a) the lattice parameters a and c, (b) the lattice parameter b and the β angle and (c) the α and γ angles as functions of temperature for the PCA crystal.

The discontinuous character of the phase transitions at 294 and 369 K is consistent with the observed changes in the unit cell parameters with temperature displayed in figures 5(a), (b) and (c) (the lattice parameters of all the phases were normalized to those found for phase I). We can notice that the phase transition at 310 K, hardly visible in the dilatometric experiment, is well evidenced by the temperature characteristic of the parameters α and β.

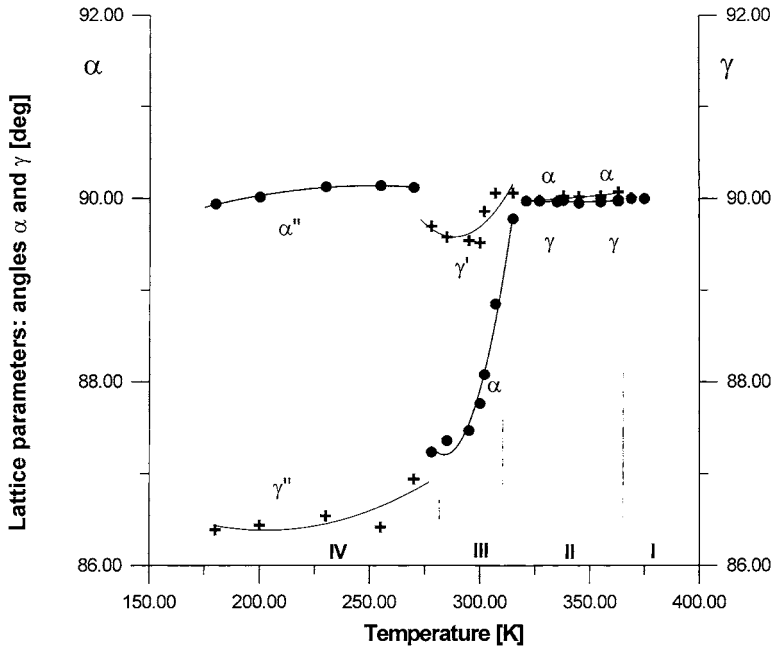

Figure 5. (Continued)

3.3. Dielectric properties

The temperature dependence of ε_c' measured between 255 and 370 K is shown in figure 6. The rapid jumps in the ε_c' value near T_{c3} and T_{c1} indicate the first-order character of the phase transitions, which is consistent with the DSC and dilatometric results. The III $\rightarrow$ II phase transition is inactive in dielectric measurements. The dielectric relaxation process is not observed in the applied range of the measuring field frequencies (75 kHz–10 MHz). The anomalies in the ε value of the order of 0.3 and 0.2 units at T_{c3} and T_{c1}, respectively, are relatively small and probably connected with the changes in the density of crystal.

Table 5. Thermodynamic parameters of the structural phase transitions in PCA (T_{PT} is the temperature of the phase transitions during a heating scan).

Phase transition	T_{PT} (K)	ΔT (K)	ΔH (kJ mol^{-1})	ΔS (J mol^{-1} K^{-1})
IV–III	294	11	2.1	7.1 (R ln 2.3)
III–II	310	0		
II–I	369	6	2.4	6.5 (R ln 2.2)

3.4. Polarizing microscope observations

The virgin sample of PCA in the room-temperature phase (phase III) usually presents a single domain. A small mechanical stress or thermal gradient creates a ferroelastic domain structure, at the same time, the (010) domain walls are dominant (see figure 7). When the III $\rightarrow$ IV phase transition is crossed one can practically observe the disappearance of the domain texture in the *a–b* plane. There are two possible explanations. First, the low temperature phase (phase IV)

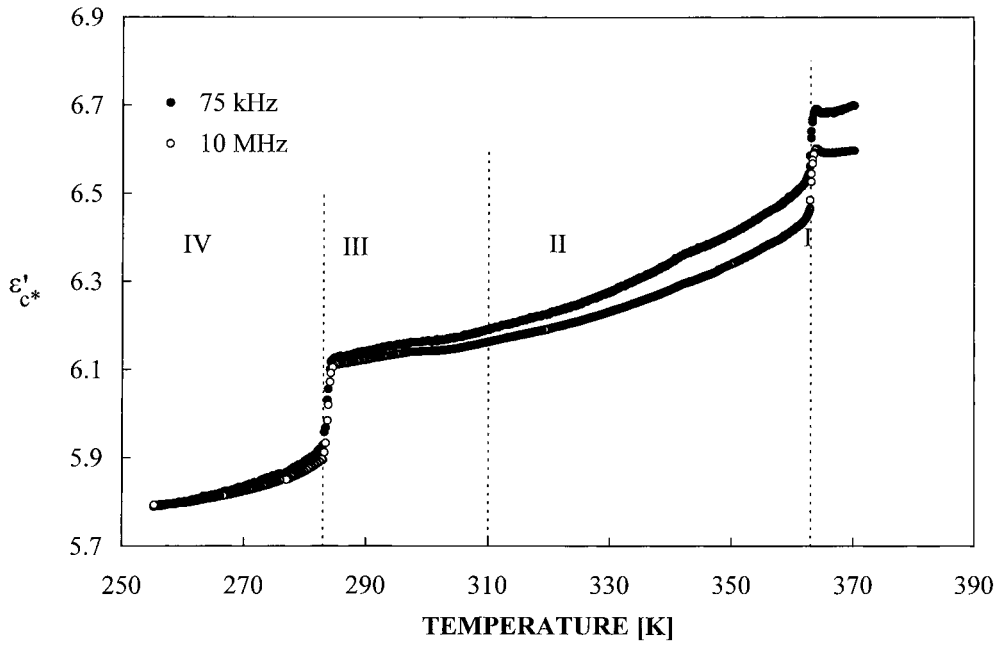

Figure 6. Temperature dependence of the real part of the complex electric permittivity ($\varepsilon^* = \varepsilon' - i\varepsilon''$) measured between 75 kHz and 10 MHz along the c^*-direction (c^* is perpendicular to the a–b plane of the triclinic phase (phase III)).

is not ferroelastic (only the traces of the ferroelastic phase (III) are fixed on imperfections or defects). Secondly, a new domain texture appears in other planes: (*bc*) or (*ac*). Approaching the ferro–paraelastic phase transition from below (1 or 2 K below 369 K) apart from the (010) domain walls, the rapid formation of the (100) ones takes place (see figure 8). Exactly at 369 K the phase front moves parallel to the *b*-axis. Next cooling of the sample from the paraelastic phase (phase I) to ferroelastic one (phase II) creates only one type of domain wall (usually (010)) without any possibility of forming (100) domains walls. The II $\rightarrow$ III phase transition, at first glance, seems not to influence the domain texture created in phase II. It should be noticed that optical observations within phase III and II were made along the c^*-direction which is perpendicular to the a–b plane. According to Sapriel [15] the ferroelastic domain structure for the $Cmcm \rightarrow Cc$ transition is expected to appear in the b–c plane. That means that the domain texture observed in our experiment is a projection of ferroelastic domains placed in the b–c plane.

3.5. Group theoretical analysis of the phase transitions in PCA

3.5.1. Paraelastic–ferroelastic (ferroelectric) phase transition at $T_{c1} = 363$ K. The paraelastic–ferroelastic (ferroelectric) phase transition of PCA at $T_{c1} = 363$ K shows a group–subgroup relation. However, the possibility of a continuous phase transition is precluded by symmetry in this case. The reason for this is that at least two irreducible representations of the paraelectric group $Cmcm$ (D_{2h}^{17}) are needed to reduce the symmetry to the ferroelectric group Cc (C_s^4). In fact there are three irreducible representations of the group $Cmcm$ (D_{2h}^{17}) which subduce the identity representation in the group Cc (C_s^4). Following the Kovalev notation, these are: τ^3, τ^6 and τ^8 [13]. Since the number of atoms per unit cell is conserved in the

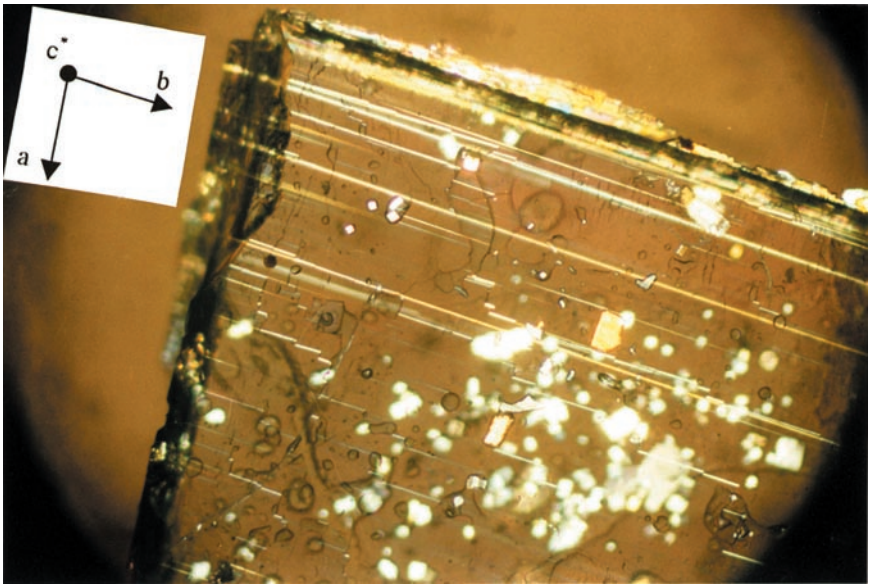

Figure 7. Ferroelastic domain structure in the *a–b* plane of the PCA crystal at 298 K (phase III).

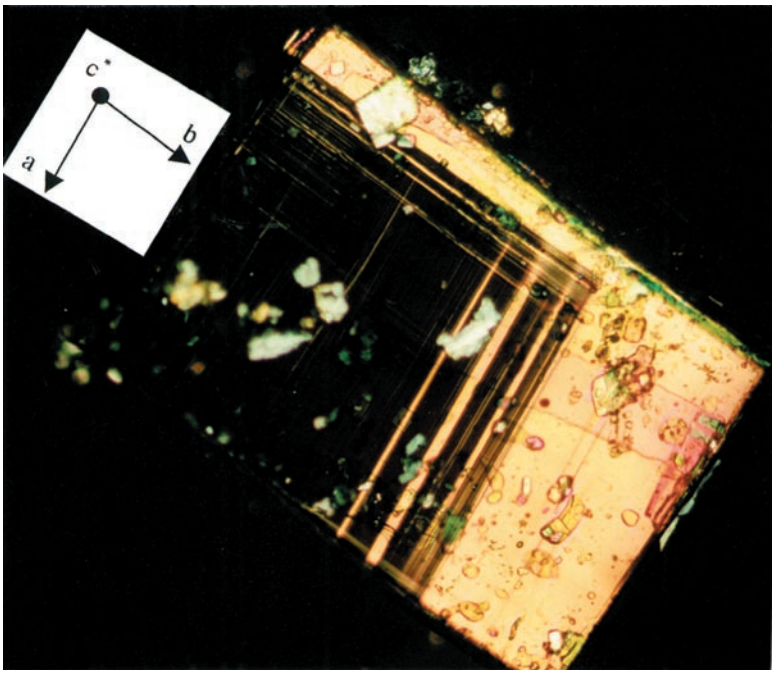

Figure 8. Ferroelastic domain structure in the *a–b* plane of the PCA crystal (phase II at 367 K) in close vicinity of the II → I phase transition (the orientation of the axis is referenced to those made for the triclinic system).

phase transition the above representations are identical with irreducible representations of the point group (factor group) *mmm* (D_{2h}). Thus the above representations are identical with

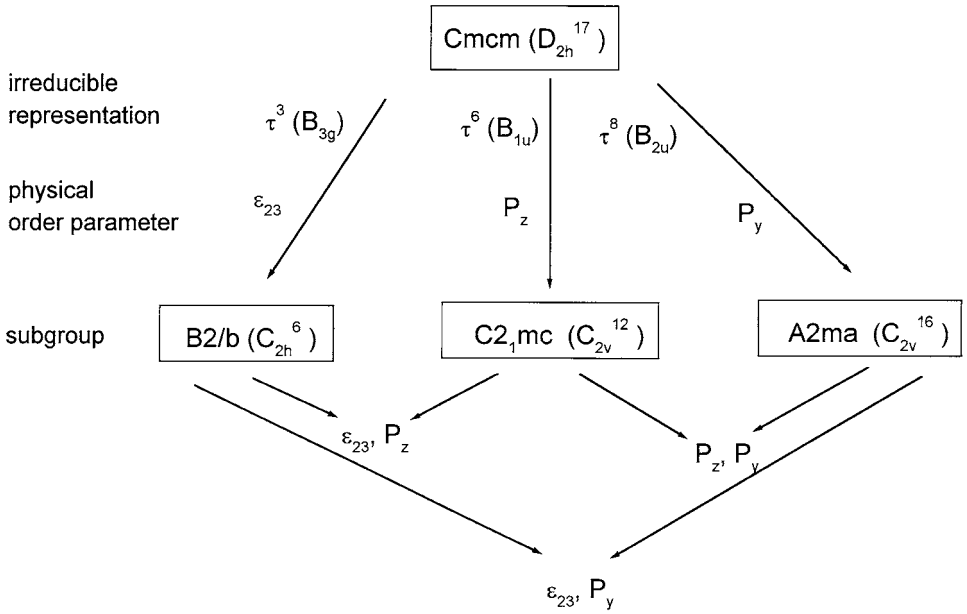

Figure 9. Scheme of symmetry reduction in the phase transition $Cmcm \rightarrow Cc$.

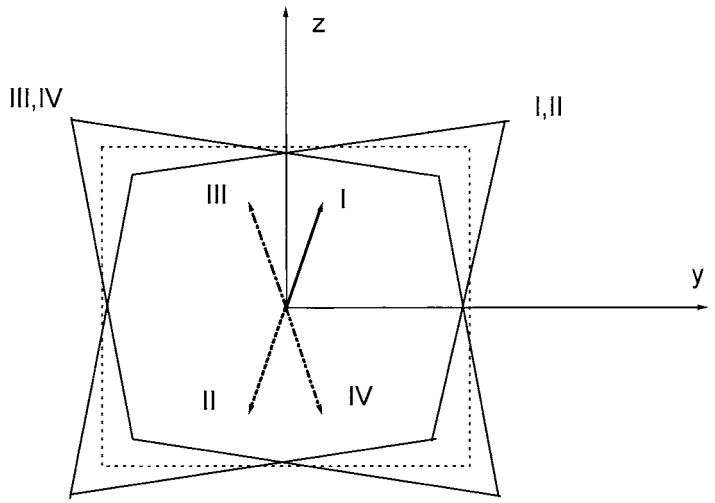

Figure 10. Polarization and shear strain in the domains of the phase Cc.

B_{3g}, B_{1u} and B_{2u} respectively. The condensation of each of these representations gives rise to a subgroup of the group $Cmcm$ (D_{2h}^{17}), which, in turn, contains the group Cc (C_s^4) as its subgroup. The scheme of this dependence is shown in figure 9. The intersection of every two of the space groups $B2/b$ (C_{2h}^6), $C2_1mc$ (C_{2v}^{12}) and $A2ma$ (C_{2v}^{16}) gives the desired ferroelectric group Cc (C_s^4). Every irreducible representation of the paraelectric group is related with a physical order parameter, which is also indicated in figure 9. The reference axes in figure 9 are defined in the tables by Kovalev [13]. Consequently, the unique axis in the group Cc (C_s^4) is parallel to the x-direction in this figure. The index of the group Cc (C_s^4) in the group $Cmcm$

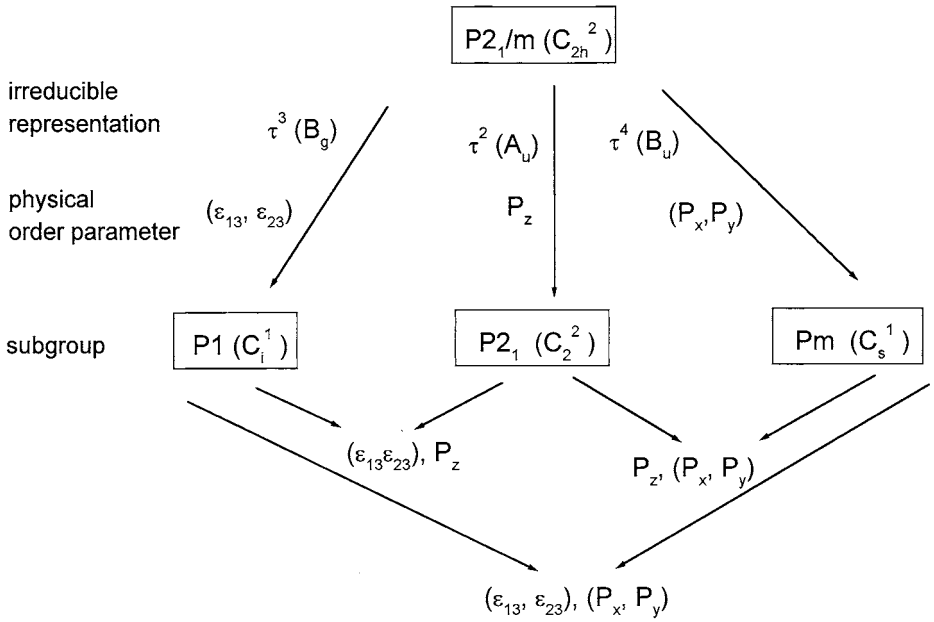

Figure 11. Scheme of the symmetry reduction in the phase transition $P2_1/m \rightarrow P1$.

Table 6. Elements of the space group $Cmcm$ in Kovalev notation; irreducible representations involved in the phase transition $Cmcm \rightarrow Cc$ and decomposition into cosets corresponding to the ferroic domains. Notice that the axis $x(100)$ of Kovalev is parallel to $y(010)$ in the crystallographic analyses. The axes y and z of Kovalev are parallel to x and z of the crystallographic analyses, respectively.

	Point element							
	h_1	h_2	h_3	h_4	h_{25}	h_{26}	h_{27}	h_{28}
Translation	000	$00c/2$	000	$00c/2$	000	$00c/2$	000	$00c/2$
τ^3	1	1	−1	−1	1	1	−1	−1
τ^6	1	−1	1	−1	−1	1	−1	1
τ^8	1	−1	−1	1	−1	1	1	−1
Domain (coset)	I	II	IV	III	II	I	III	IV

(D_{2h}^{17}) being four means that there are four orientational domains of the ferroelectric phase [14]. These domains are schematized in figure 10 in the same reference system. The components of the spontaneous polarization lie in the plane ⟨100⟩ as well as the axes of the deformation ellipsoid of the spontaneous strain. The domains I and II have the same spontaneous strain. The same concerns domains III and IV. The values of the components P_y and P_z are not determined by symmetry. In figure 11 we have tentatively assumed $P_z > P_y$. The stress-free domain boundaries may appear in the planes ⟨010⟩ and ⟨001⟩ [15]. Since there is no symmetry operation in the group $Cmcm$ (D_{2h}^{17}), which would transform these orientations into each other, the domain boundaries are not energetically equivalent. Moreover, if the P_y and P_z components are not equal the system seems to adopt preferentially the domain walls characterized by, as much as possible, antiparallel polarizations. This means that the domain wall I–IV should be preferred over I–III, etc. Switching between domains I and III or II and IV does not change the

Table 7. Regions of stability, symmetries and lattice parameters of phases of PCA.

	Phase			
	IV	III	II	I
T_c (K)		283	310	363
T (K)	175	293	338	378
a (Å)	7.941(2)	8.013	7.999	7.741
b (Å)	7.965(2)	8.042	22.569	22.576
c (Å)	11.435(2)	11.917	8.139	8.142
α (°)	90.00(3)	89.51	90.0	90.0
β (°)	106.66(3)	70.58	96.46	90.0
γ (°)	90.00(3)	82.97	90.0	90.0
Space group	$P2_1/m$	$P1$	Cc	$Cmcm$

deformation whereas switching between I $\rightarrow$ III, I $\rightarrow$ IV, II $\rightarrow$ III and II $\rightarrow$ IV is also related with a shear. Thus, group theory predicts the possibility of the switching of polarization by an external stress and the switching of deformation by an external electric field. The irreducible representations involved in the phase transition I $\rightarrow$ II and the cosets corresponding to the domains are gathered in table 6. Denoting by η_1, η_2 and η_3 the order parameters related with the representations τ^3, τ^6 and τ^8 respectively, one can write the Landau free energy expansion:

$$F(\eta_1, \eta_2, \eta_3; T) = \frac{1}{2}\left(\sum_{i=1}^{3} A_i \eta_i^2\right) + B\eta_1\eta_2\eta_3 + \frac{1}{4}\left(\sum_{i=1}^{3} C_i \eta_i^4 + \sum_{i=1, j>i}^{3} \tilde{C}_{ij}\eta_i^2\eta_j^2\right) + \eta_1\eta_2\eta_3$$
$$\times \sum_{i=1}^{3} D_i\eta_i^2 + E_{222}\eta_1^2\eta_2^2\eta_3^2 + \sum_{i=1}^{3} E_{600}\eta_i^6 + \sum_{i,j=1}^{3} \tilde{E}_{ij}\eta_i^4\eta_j^2 \ldots . \quad (1)$$

The above expansion is given up to the sixth order although for the simplest description it is enough to terminate it on the fourth-order term provided that it is positive definite. The presence of the odd terms (B and D) makes it so that the phase transition cannot be continuous. The leading temperature dependence is usually put into one of the coefficients A_i. Experiment can reveal this dependence: a softening is expected in the z- or y-component of the dielectric susceptibility or in the shear elastic constant C_{44}. The unique plane (010) of the domain walls is seen in the polarization microscopy patterns (figure 8). The texture visible in the $Cmcm$ phase is more difficult to explain. It may be a result of growth of the $Cmcm$ phase on the well defined matrix of the Cc phase. Alternatively it can be regarded as a ferroic domain system originating from a paraphrase of still higher symmetry.

3.5.2. Phase transition at 310 K. From table 7 it follows that the phase transition II $\rightarrow$ III does not exhibit a group–subgroup relation. The point symmetry operations are all lost but a lattice translation is gained when the temperature is lowered. This is characteristic of martensitic phase transitions [16]. Such phase transitions are, in principle, discontinuous, but the formation of the new phase may take quite a long time. It is important that there is a strict relation of the orientation of the new phase with respect to the old phase. A strong shear ε_{23} related with the angle α suggests that the one of the planes (010) or (001) in phase II may be the plane of shuffling in the martensitic phase transition. We are now in search for polarizing microscopy patterns corresponding to the coexistence of phases. The thermal effect suggesting a continuous phase transition may results from slow kinetics of the transition.

Table 8. Elements of the group $P2_1/m$ in Kovalev notation; irreducible representations involved in phase transition $P2_1/m \rightarrow P1$; and decomposition into cosets corresponding to the ferroic domains.

	Point element			
	h_1	h_4	h_{25}	h_{28}
Translation	000	$00c/2$	$00c/2$	000
τ^2	1	1	−1	−1
τ^3	1	−1	1	−1
τ^4	1	−1	−1	1
Domain (coset)	I	II	III	IV

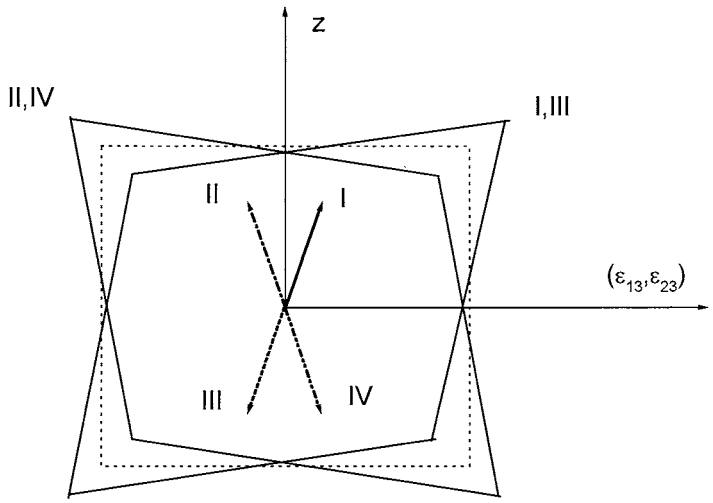

Figure 12. Polarization and shear strain in the domains of the phases $P1$ as resulting from a phase transition from phase $P2_1/m$.

3.5.3. Phase transition at 283 K. The phase transition III → IV shows a group–subgroup relation, but interesting enough the higher-symmetry phase, phase IV, appears at lower temperature. The symmetry breaking $P2_1/m(C_{2h}^2) \rightarrow P1(C_1^1)$ is also related with multiple representations. The representations are given in table 8. Figure 11 shows the scheme of the symmetry reduction in the phase transition $P2_1/m \rightarrow P1$ (IV → III) and the corresponding physical order parameters. As the phase transition is equitranslational, the irreducible representations are equivalent to the representations of the point group $2/m$ (factor group). Figure 12 represents the spontaneous strain and a projection of the spontaneous polarization onto the plane $(\varepsilon_{13}, -\varepsilon_{13}, 0)$. The stress-free ferroelastic domain boundaries are oriented along the planes (001) and $(\varepsilon_{13}, \varepsilon_{13}, 0)$ in the reference system of phase IV. The Landau expansion of the free energy has the same form as that given in equation (1).

4. General discussion

Both the $RSbC_6$ and $RSbCl_6 \cdot RCl$-type crystals are characterized, in general, by quite a simple crystal structure. They are composed of isolated octahedral units $SbCl_6^-$ and organic

cations (R). In the case of $RSbCl_6 \cdot RCl$ analogues, isolated Cl^- anions also appear in the crystal lattice. The organic cations are stabilized in the crystal lattice by rather weak N–H $\cdots$ Cl hydrogen bonds (3.2–3.4 Å). In the case of $RSbCl_6$ crystals the organic cations are connected to the Cl atoms belonging to the Sb coordination sphere, whereas for $RSbCl_6 \cdot RCl$ the N–H $\cdots$ Cl hydrogen bond formed with the isolated Cl^- anions are preferred. In the last case the hydrogen bonds are stronger and therefore the freedom of motion of the cations is distinctly restricted. Since the organic and $SbCl_6^-$ units are isolated in the crystal lattice both of these forms may contribute to the 'order–disorder' mechanism of structural phase transitions. This may justify the complex sequence of phase transitions for several of them. The phase situation discovered up to now in the ferroic $RSbCl_6$ crystals is presented in table 9. Excluding from the comparison the $(C_5H_{10}NH_2)SbCl_6 \cdot (C_5H_{10}NH_2)Cl$ crystal, it is interesting to notice that para–ferroelastic phase transition, independently of the type of organic cation, takes place in the approximate temperature range. The dielectric response of those crystals reveals considerable similarity, showing an abrupt decay in the dielectric permittivity value in the vicinity of the phase transitions. The shape of the dielectric anomaly, typical for crystals having a so-called 'rotator phase', is connected with the rapid freezing of rotational motion of organic cations. A small value of the electric permittivity results from the fact that dipole–dipole interactions, within the cationic sublattice or between cationic and anionic units are quite weak.

Table 9. Structural phase transitions in ferroic chloroantimonate (v) crystals. (P denotes paraelastic and F denotes ferroelastic).

Crystal	Temperature (K) (and order of the phase transition)	Symmetry	Character of the phase transition	ΔS (J mol^{-1} K^{-1})
$[P(CH_3)_4]SbCl_6$	405 (first)	$? \rightarrow C2/m$	P–P	47.8
	350 (second)	$C2/m \rightarrow P\bar{1}$	P–F	—
$[C(NH_2)_3]SbCl_6$	351 (first)	hexagonal $\rightarrow 2/m$	P–F	24.2
	265 (second)	$C2/m \rightarrow P2_1/a$	F–F	—
$[(C_2H_5)_3NH]SbCl_6$	336 (first)	$C222 \rightarrow P2_1/n$	P–F	25.9
$(C_5H_{10}NH_2)SbCl_6 \cdot (C_5H_{10}NH_2)Cl$	202 (second)	$Pccn \rightarrow P2_1/c$	P–F	—
$(C_5H_{10}NH_2)SbCl_6$	369 (first)	$Cmcm \rightarrow Cc$	P–F	6.5
	307 (second)	$Cc \rightarrow P1$	F–F	—
	294 (first)	$P1 \rightarrow P2_1/m$	F–P?	7.1

Taking into account the ferroic crystals considered above and containing dipolar piperidinium cation, $(C_5H_{10}NH_2)SbCl_6$ and $(C_5H_{10}NH_2)SbCl_6 \cdot (C_5H_{10}NH_2)Cl$, a distinct difference in their dielectric properties seems to be connected not only with different anionic sublattices but, mainly, with the dynamics of the piperidinium cations. A large value of the dielectric permittivity and clear relaxation process revealed over the paraelastic phase of $(C_5H_{10}NH_2)SbCl_6 \cdot (C_5H_{10}NH_2)Cl$ were explained in terms of reorientational motion (the puckering between two chair conformations) of the dipolar piperidinium cation. Our x-ray measurements of $(C_5H_{10}NH_2)SbCl_6$ show that the III $\rightarrow$ II phase transition leads to the change of the conformation from chair to the twisted boat. Since such a change of conformation is connected with an insignificant shift of one of the C atoms, such motion does not lead to an important change in the resultant dipole moment of the unit cell. As a result, the discussed phase transition may be accompanied by only a subtle dielectric anomaly. The proposed mechanism of phase transition in PCA is analogous to that found in a closely related compound, namely $(C_5H_{10}NH_2)_2SbCl_5$ [17]. The dielectric response recorded for PCA at 310 K and $(C_5H_{10}NH_2)_2SbCl_5$ at 339.5 K show great similarity. On the other hand it is necessary to

take into account also the contribution of the $SbCl_6^-$ group to the mechanism of III $\rightarrow$ II phase transition. X-ray data show that one of the chlorine atoms (Cl(6)) is split between two positions, which indicate the disordering of the anion groups in phase II. We were not able to determine the type of disorder of the piperidinium cation in the paraelastic phase (phase I). Taking into account the fact that dielectric anomaly at the II $\rightarrow$ I phase transition is subtle, one can expect, at the outmost, a libration of the piperidinium ring in the *a–b* plane in the paraelastic phase. The beginning of such a motion is suggested to exist over phase II, for which large thermal parameters of the C and N(1) atoms of the piperidinium ring were found. To verify the molecular mechanism of the phase transitions in PCA crystal ^{1}H-NMR studies are now in progress.

Formal group theoretical analysis predicts the first-order character and the polar properties of the $Cmcm \rightarrow Cc$ phase transition as well as the $P2_1/m \rightarrow P1$ phase transition. The same theory also explains correctly the orientation of the ferroelastic stress-free domain walls in phase II. An experimental determination of the order parameters of section 3.5.1 would require dielectric measurements in different spatial directions. Unfortunately, our dielectric measurements were performed for the direction perpendicular to the *a–b* plane only since we did not succeed in obtaining good-quality single crystals large enough to be able to prepare the samples cut perpendicular to the *a* and *b* axes. The domain structure of phase III is a result of a ferroelastic phase transition (IV $\rightarrow$ III). Detailed structural studies are still needed to reveal the origin of the apparently continuous character of the phase transition II $\rightarrow$ III where a group–subgroup relation does not hold.

5. Summary

X-ray diffraction studies at 338 and 293 K showed that the structure of $RSbCl_6$ crystal consists of isolated $SbCl_6$ units and piperidinium cations. In the room-temperature phase (293 K) both cations and anions are ordered, whereas above 307 K they exhibit relatively large temperature factors (especially the C and Cl(6) atoms). The temperature dependent x-ray studies revealed the following sequence of the phase transitions:

$$\begin{array}{lll} 363\ \mathrm{K} & 310\ \mathrm{K} & 283\ \mathrm{K} \\ Cmcm(\mathrm{I}) \rightarrow & Cc(\mathrm{II}) \rightarrow & P1(\mathrm{III}) \rightarrow P2_1/m(\mathrm{IV}). \end{array}$$

Structural phase transitions were investigated using differential scanning calorimetry, dilatometric and optical observations. The I $\rightarrow$ II and III $\rightarrow$ IV phase transitions were found to be strongly of first order, whereas the II $\rightarrow$ III transition was second order. The optical observations showed that the ferroelastic domain structure appear below 363 K. The mechanism of the phase transitions is believed to be connected with the dynamics of both the $SbCl_6^-$ anions and the $C_5H_{10}NH_2^+$ cations.

Acknowledgments

This work was supported by the Polish State Committee for Scientific Research (project register 3 TO9A 058 17).

References

[1] Jakubas R and Sobczyk L 1990 *Phase Trans.* **20** 163

[2] Ishihara H, Watanabe K, Iwata A, Yamada K, Kinoshita Y, Okuda T, Krishnan V G, Dou S and Weiss A 1992 *Z. Naturforsch.* A **47** 65

[3] Kozioł P, Furukawa Y and Nakamura D 1991 *J. Phys. Soc. Japan* **60** 3850
[4] Sobczyk L, Jakubas R and Zaleski J 1997 *Polish J. Chem.* **71** 265
[5] Jakubas R, Krzewska U, Bator G and Sobczyk L 1988 *Ferroelectrics* **77** 129
[6] Zaleski J, Pawlaczyk Cz, Jakubas R and Unruh H-G 2000 *J. Phys.: Condens. Matter* **12** 7509
[7] Ciapała P, Jakubas R, Bator G, Pietraszko A and Kosturek B 1998 *J. Phys.: Condens. Matter* **10** 5439
[8] Jakubas R, Ciapała P, Pietraszko A, Zaleski J and Kusz J 1998 *J. Phys. Chem. Solids* **59** 1309
[9] Bednarska-Bolek B, Pietraszko A, Jakubas R, Bator G and Kosturek B 2000 *J. Phys.: Condens. Matter* **12** 1143
[10] Bednarska-Bolek B, Ciunik Z, Jakubas R, Bator G and Ciapała P *J. Phys. Chem. Solids* submitted
[11] Sheldrick G M 1993 *SHELXL, Program for Crystal Structure Refinement* University of Goettingen, Germany
[12] Sheldrick G M 1997 *SHELXL, Program for Crystal Structure Refinement* University of Goettingen, Germany
[13] Kovalev O V 1965 *Irreducible Representations of the Space Groups* (New York: Gordon Breach)
[14] Zieliński P 1990 *Surf. Sci. Rep.* **11** 179
[15] Sapriel J 1975 *Phys. Rev.* B **12** 5128
[16] Roitburd A L 1978 *Solid State Phys.* **33** 331
[17] Bednarska-Bolek B, Zaleski J, Jakubas R and Bator G 2000 *J. Mol. Struct.* **553** 175